HALL EFFECT IN A PLASMA

DYLAN R. NELSON

Department of Physics, University of California, 366 LeConte Hall, Berkeley, CA 94720-7300: `dnelson@berkeley.edu`

PARTNERS: JOEY CHEUNG, PAUL HIGGINS

Department of Physics, University of California, 366 LeConte Hall, Berkeley, CA 94720-7300: `jpc168@berkeley.edu`, `phiggins@berkeley.edu`

ABSTRACT

The Hall effect is observed in a low-density, weakly ionized plasma discharge tube. The relatively low number density of charge carriers in such an environment enables observation of the effect and characterization of the plasma environment. First, we determine the response of the magnet field to applied magnetic current, and discover a weak though evident hysterisis effect. We measure the Hall voltage drop across the diameter of the helium filled tube as a function the electrical, magnetic, and gas parameters under our experimental control. From these measurements we calculate the electron drift velocity, number density, collision frequency, effective temperature, and average energy. The functional dependence of these plasma parameters on the applied voltage between the two ends of the discharge tube as well as the strength of the applied magnetic field are investigated. Finally, we consider the role of dynamical instabilities in the plasma, and comment on the interactions between free electrons, ions, and their environment.

Subject headings: Hall effect; discharge columns; plasma instabilities; magnetic hysterisis; ionization phenomena

1. INTRODUCTION

The Hall effect results from an asymmetry of charge distribution in a conducting media when a magnetic field is applied perpendicular to the motion of charge carriers. The Lorentz force acts to separate positive and negative charges, in turn establishing a potential difference and so an electric field perpendicular to both the current flow and the applied magnetic field. This effect can be measured experimentally as a "Hall voltage" difference between the extremes of this charge separation.

Classically, the Hall effect was used to determine the sign of charge carriers. In fact, it was one of the first experiments supporting the idea that current in metals is carried by negatively charged electrons and not positively charged protons. The Hall effect also enables a direct way to determine several properties of the conducting medium. The drift velocities and densities of charge carriers can be determined, along with the collision frequency and the effective temperature associated with the carrier velocity distribution. Alternatively, the Hall effect is often used to measure the strength of an external magnetic field, if detailed properties of the medium in which it is measured are already known.

However, the magnitude of the Hall effect in typical conducting metals is quite small. Its amplitude is inversely proportional to the number density of charge carriers, that is, $V_H \propto n_q^{-1}$. In metals, n_q is of order 10^{29} m^{-3}, while in semiconductors and many plasmas n_q is several orders of magnitude smaller. Therefore, the effect is much more pronounced in both semiconductors and low-density plasmas which have comparatively low densities of charge carriers. We exploit this fact to measure the Hall voltage across a helium discharge column as a function of magnetic field strength, discharge current in the plasma, and gas pressure. We begin in §2 with a brief review of the plasma physics relevant to such a

gas discharge column. §3 covers the apparatus, experimental procedure, and measurements conducted, while §4 offers analysis of the results and the calculation of relevant plasma properties.

2. THEORY

2.1. *Hall Effect*

In the case of a single type of charge carrier, the electric current in a normal conductor can be described macroscopically or microscopically. Given a number density n_q of charge carriers each with charge q moving with a drift velocity $\boldsymbol{u}_q$ the current density is given by

$$\boldsymbol{j} = q n_q \boldsymbol{u}_q. \tag{1}$$

The macroscopic current $\boldsymbol{I}$ is then

$$\boldsymbol{I} = \boldsymbol{j} A, \tag{2}$$

where A is the cross-sectional area of the conductor. The "Hall field" $\boldsymbol{E}_H$ is defined to be

$$\boldsymbol{E}_H \cong -\boldsymbol{u}_q \times \boldsymbol{B} = \boldsymbol{B} \times \boldsymbol{j} / q n_q. \tag{3}$$

Here, $\boldsymbol{B}$ is the external magnetic field. We can see how this arises by explaining the resistivity of a conductor as the friction between charge carriers and the background medium. Defining a frictional force

$$\boldsymbol{F}_f = -m_q \nu_q \boldsymbol{u}_q \tag{4}$$

where ν_q is the collision frequency, i.e., the number of collisions per second on average whereby the charge carrier imparts its momentum $m_q \boldsymbol{u}_q$ to the medium. For force balance we must also take into account the electric and magnetic forces on a mobile charge carrier, given by the Lorentz force law as

$$\boldsymbol{F}_L = q\boldsymbol{E} + q\boldsymbol{v} \times \boldsymbol{B} = q\boldsymbol{E}_o + q\boldsymbol{u}_q \times \boldsymbol{B}. \tag{5}$$

The Lorentz force causes the separation of charge resulting in the internal Hall field. We call $\boldsymbol{E}_o$ the "Ohmic" electric field, which can be expressed as

$$\boldsymbol{E}_o = \eta\boldsymbol{j} = \left(\frac{n_q\nu_q}{m_q q^2}\right)\boldsymbol{j} \tag{6}$$

where η, the resistance, is as given. Given the frictional force of (4) and the Lorentz force of (5), there is one additional force $\boldsymbol{F}_H = q\boldsymbol{E}_H$ corresponding to the Hall field. Then, force balance for steady state gives $\boldsymbol{F}_f + \boldsymbol{F}_L + \boldsymbol{F}_H = 0$, or

$$-m_q\nu_q\boldsymbol{u}_q + q\boldsymbol{E}_o + q\boldsymbol{u}_q \times \boldsymbol{B} + q\boldsymbol{E}_H = 0. \tag{7}$$

This is Ohm's law for a total electric field $\boldsymbol{E} = \boldsymbol{E}_o + \boldsymbol{E}_H$ incorporating the Hall effect. Equation (7) justifies the definition of the Hall field proposed in (3).

2.2. *Non-uniform Carrier Density*

The above treatment is valid only in the case of a uniform density of charge carriers. However, in the case of the cylindrical gas discharge column used in this experiment, the density distribution peaks near the center and falls to zero at the edges, as in Figure (1).
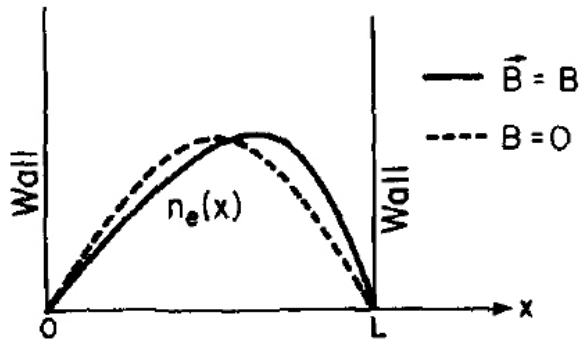

Fig. 1.— Density distribution of charge carriers (electrons) in a glow discharge column. The dashed line is without any external magnetic field, while the solid line is in the presence of a $\boldsymbol{B}$ field perpendicular to the current direction. Both show a centrally peaked distribution that falls off towards the edges of the column. Image from Kunkel, 1980.

This can be verified visually as the gradual decrease in intensity of the pink discharge glow. The non-uniformity leads to a pressure gradient, requiring the inclusion of a fourth force in our steady state equation (7) given by

$$\boldsymbol{F}_\rho = -\nabla P = -\nabla n_q k T_q \tag{8}$$

arising from the ideal gas law, where T_q is the temperature of the charge carriers. By assuming a one-dimensional geometry, previous work (Kunkel, 1980) found the charge density distribution to be given by

$$n_e(x) = n_o \exp\left(-ax/2\right)\sin\left(x/\Lambda\right) \tag{9}$$

where $\Lambda = L/\pi$ is the diffusion length, and $n_e(x)$ is roughly as shown in Figure (1). The voltage drop can be calculated as the line integral of the electric field across the width of the one-dimensional column, i.e.

$$\Delta V_H(x_1, x_2) \equiv \int_{x_1}^{x_2} E_x dx \tag{10}$$

$$= \frac{(x_2 - x_1)}{2}E_H. \tag{11}$$

The result is that, if x_1 and x_2 are taken equidistant from the midpoint of the column, as in our experiment, then the "ambipolar" field $\boldsymbol{E}_\rho$ associated with the force in (8) cancels exactly half of the Hall field, as previously mentioned.

2.3. *Plasma Discharge*

Starting from eqns. (1)-(6), simple manipulation gives the drift velocity and number density of charge carriers in terms of measured electrical parameters and $\boldsymbol{E}_H$ as

$$u_q = \frac{\boldsymbol{E}_H}{B} = \frac{V_H \Delta x}{B} \tag{12}$$

and

$$n_q = \frac{I_d B}{qAE_H}. \tag{13}$$

The collision frequency ν_q is given by

$$\nu_q = \left(\frac{\boldsymbol{E}_o}{\boldsymbol{E}_H}\right)\Omega_q, \tag{14}$$

where $\Omega_q = qB/m_q$ is the cyclotron frequency of the charge carriers. $\Omega_e \simeq 2 \times 10^{11}\,B$ (Tesla) for electrons, which we use later in order to determine a characteristic temperature for the free electrons in the plasma.

3. MEASUREMENTS

3.1. *Apparatus*

The equipment setup used in this experiment is shown schematically in Figure (2). We operate the glow discharge column at low pressures, between 15 and 30 torr, with a gas mixture composed primarily of helium, with 1% argon and 0.1% argon. The argon has the lowest ionization energy and provides the majority of free electrons for the plasma, while the nitrogen helps prevent contamination by impurities.

We operate at discharge currents between 0.1 and 2.5 mA, with high discharge voltages between 0 and 3,000 V. Fluctuations caused by wave phenomena, striations, and other instabilities are monitored by an oscilloscope attached to the grounded probe. Stable conditions are prerequisite to precise measurements, and we require voltage oscillations $\leq 0.1V$, achieved by balancing gas flow rate and discharge current, especially at low pressures.

The discharge potential maintained across the electrodes on either end of the tube causes charges to accelerate and collide, ionizing additional atoms and creating populations of free electrons and ions. Together with recombination occurring primarily at the tube walls, a steady state is established resulting in a constant current flow through the plasma tube. By using a variable amplitude magnetic field, measurements of the Hall effect can determine the parameters of the plasma.
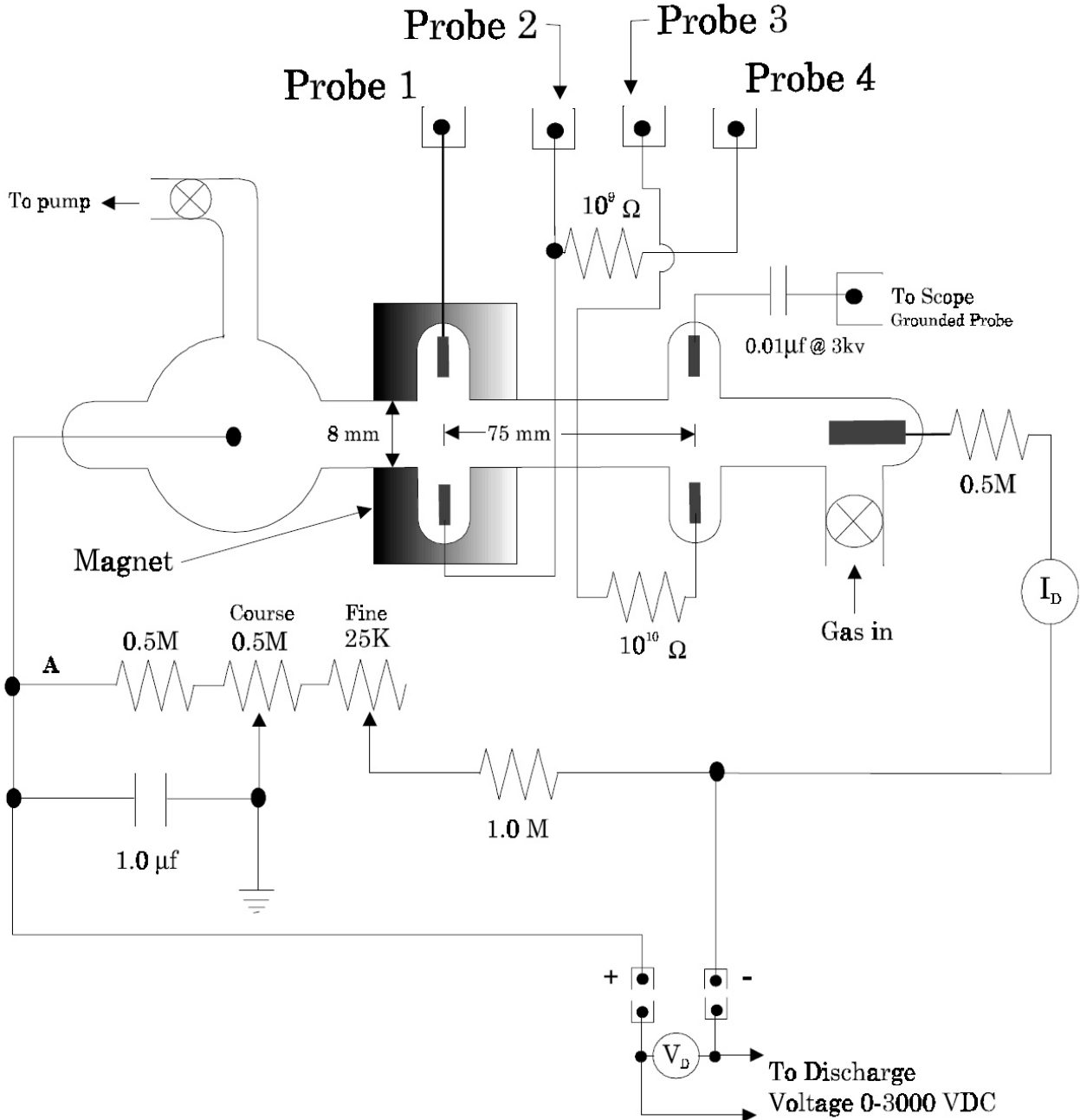
FIG. 2.— Schematic diagram of the apparatus used in this experiment. The discharge electronics and points of measurement for I_d and V_d are shown, as well as the four fixed probes used to measure voltage differences in the plasma column. The potentiometer bridge arrangement allows the probes to be kept close to a floating ground potential. Not shown is the control circuit for the electromagnet, which is controlled by adjusting the "magnetic" current I_M.

3.2. Observations

First, to illustrate the resistive properties of a plasma discharge, we measure the discharge voltage V_o as a function of discharge current I_d. The discharge voltage is given across probes 2 and 3 in Figure (2), and both quantities are controlled by changing the high voltage potential between the two ends of the gas discharge tube. We also repeat the measurement series for gas pressures between 15 and 30 torr in increments of 3 torr, in order to characterize the plasma response with pressure. The results are given in Figure (3).

This result highlights the atypical relation between current and voltage in a plasma discharge. Instead of an Ohmic relation similar to $V = IR$ which we might expect from a metal conductor, the discharge voltage is found to be independent, to within error, of the discharge current. This relation is true independent of pressure, although the overall voltage level does increase linearly with pressure. Since increased pressure means a higher number density of charge carriers, the plasma requires a higher voltage to discharge.

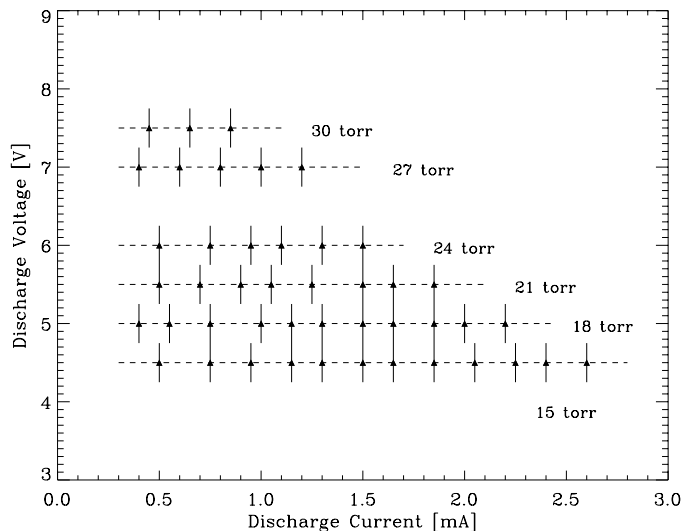Next, we characterize the magnetic field produced as

FIG. 3.— Discharge voltage as a function of discharge current for six different gas pressures from 15 to 30 torr. The response is decidedly non-Ohmic. In fact, voltage across the probes is found to be roughly independent of increasing current, for all pressure settings. Error in I_D is estimated to be ± 0.05 mA, and error in V_o is estimated to be ± 0.25 V.

a function of the magnetic current I_M. The detector probe of a gaussmeter was fixed in a vertical orientation between the two poles of the magnet. The exact position of the probe was adjusted to find the maximum field strength for a specific current, and then fixed in place. We measure field response from -2.3 to +2.3 A of current in 0.1 A increments. The maximum magnetic field strength recorded was $\simeq 595$ G, with good linearity as evidenced in Figure (4).
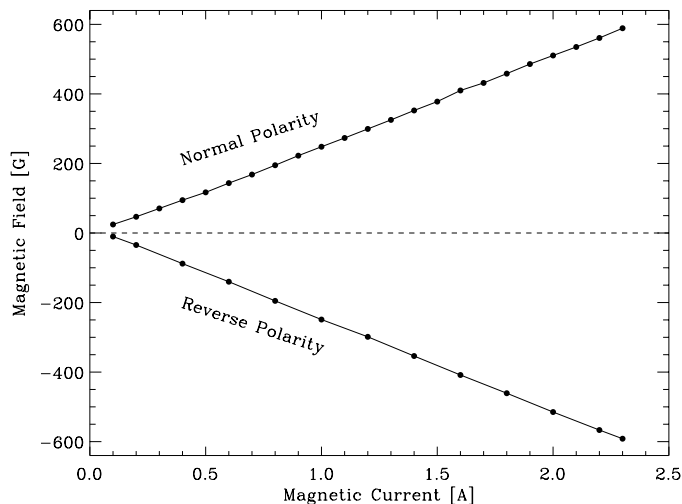

FIG. 4.— Magnetic field strength B as a function of magnetic current I_M, for both normal and reverse polarity. The two curves were fit with linear relations of $B_n = 259.2 I_M - 9.4$ and $B_r = 265.7 I_M + 17.9$, respectively. The unreduced χ^2 goodness-of-fit statistics are 1.9e3 and 1.8e3, respectively.

The difference of y-intercept for the normal and reverse polarity fits is $\simeq 27$ G, and is indicative of a small hysterisis effect in the magnet. To better quantify this effect and possible errors incurred as a result, we traced the magnetic field strength continuously, starting from zero current, up to the maximum, and back to zero. The

polarity was then reversed, and taken down to the maximum negative current, and finally back to zero again. The results are given in Figure (5), in which the characteristic signature of a ferromagnetic material is present.
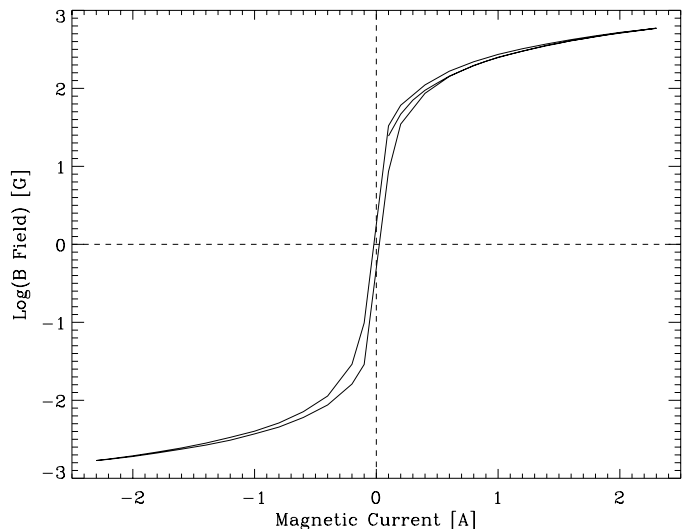

FIG. 5.— Magnetic field strength B measured as a continuous function of magnetic current I_M. By slowing varying the current through both the positive and negative ranges, the hysterisis curve can be seen.

Hysterisis in this case results from the alignment of ferromagnetic domains in the iron dielectric used to increase the strength of the magnet. In effect, they "remember" the history of applied magnetic fields, and reducing the current to zero will not in general reduce the magnetic field to zero. To zero the field, an AC current should be applied and slowly reduced to zero. However, for the purposes of this experiment, the hysteric effect is minimal and will for the most part be disregarded.

Finally, we measured the Hall field $\boldsymbol{E}_H$ as a function of magnetic field strength. As before, we repeat the process over a range of pressures to examine any functional dependence. The Hall voltage V_H can be measured directly between probes 1 and 2. The voltage is converted to the Hall field in units of $V\,m^{-1}$ by using (10). We take measurements for the full range of magnet current (and therefore $\boldsymbol{B}$ fields), adjusting the potentiometer bridge after each change of parameters to keep the probes floating near ground potential. The results are shown in Figure (6).

We expect a linear relation between the Hall field and applied magnetic field, at least in the low field limit (≤ 300 G). Linearity extends well beyond this point, however, with $\boldsymbol{E}_H$ increasing with B. Deviation at high magnetic fields is likely due to induced distortions of the discharge, e.g., the distribution of charge carriers. This may result when the magnetic field invalidates the axial symmetry assumption. To quantify the goodness-of-fit, we plot the residuals between the measured points and theoretical line in Figure (7).

For the most part, deviation is at most 30 G, and is generally less with increasing pressure. This is not overly concerning since the errors associated with absolute measurement of the magnetic field due to hysteresis are of order the same magnitude. Furthermore, an error level of $\simeq 30\%$ is expected with laboratory plasma experiments of
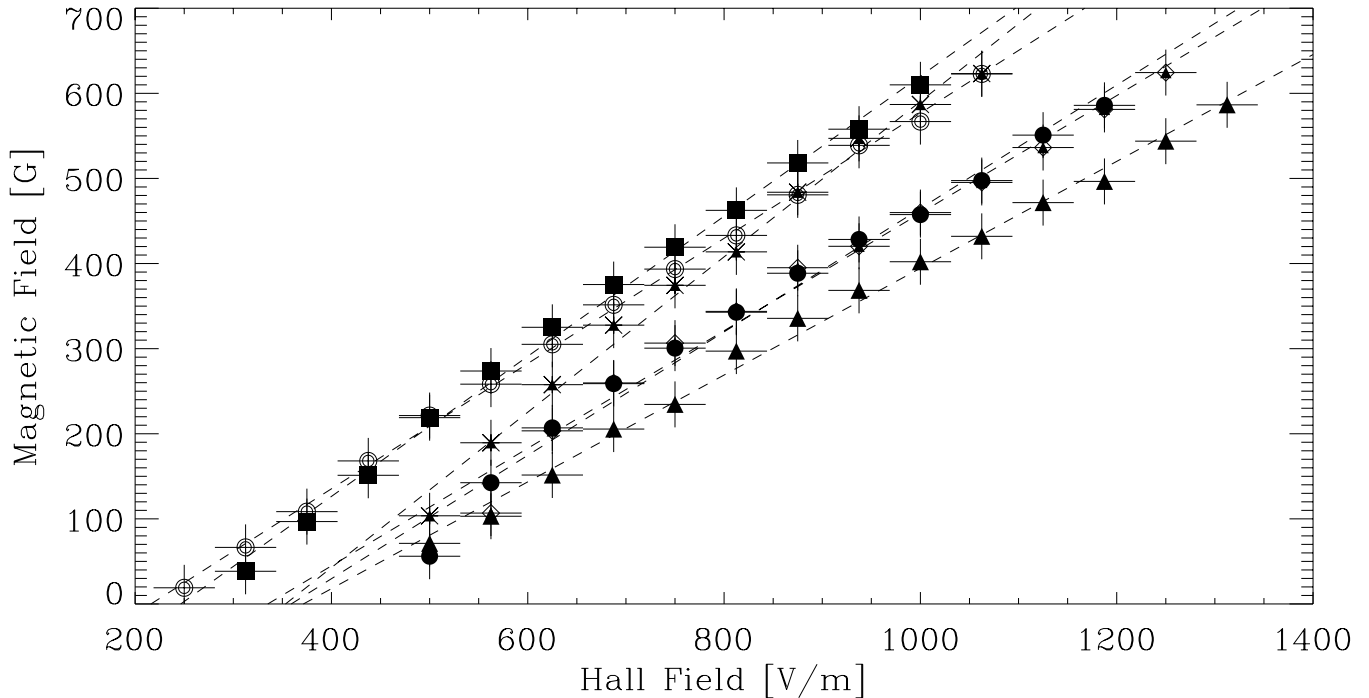
FIG. 6.— Magnitude of the Hall field $\boldsymbol{E}_{\mathrm{H}}$ as a function of magnetic field strength, over the full range of current values. Measurements are made at pressures corresponding to 15, 18, 21, 24, 27, and 30 torr. These correspond to stars, empty diamonds, filled circles, filled triangles, filled squares, and empty circles, respectively.
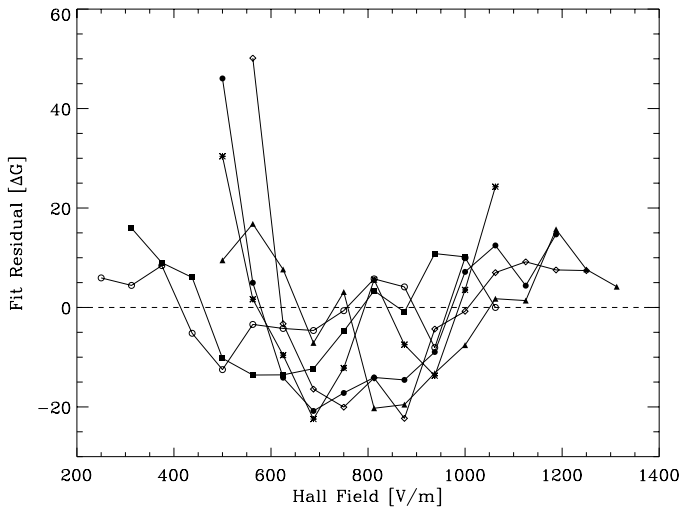

FIG. 7.— Residuals of the linear fit for $\boldsymbol{E}_{\mathrm{H}}$ as a function of B, the magnetic field strength. The symbols correspond to different pressure values, and are as described in the caption of Figure (6).
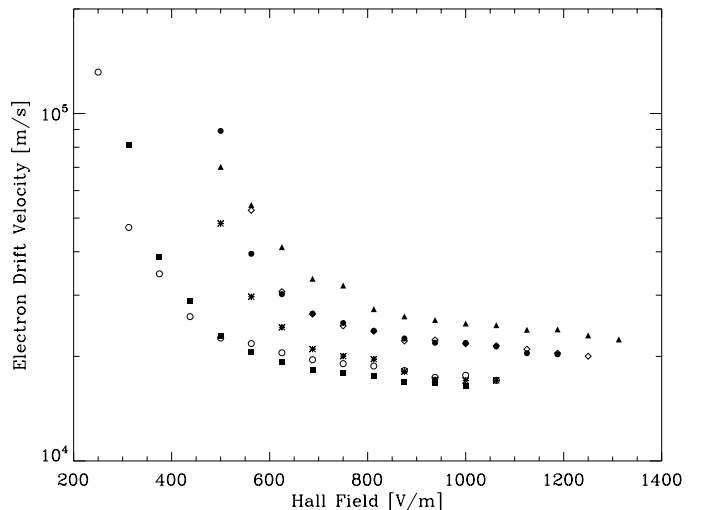

FIG. 8.— Electron drift velocity as a function of the Hall field. Maximum measured values are approximately 15,000 m/s, in good agreement with typical values we expect for the setup. Velocities decrease with increasing Hall fields, independent of any change in pressure.

this type. With this relation established, we can proceed to calculate several properties of the plasma and compare with theoretical predictions.

4. RESULTS AND DISCUSSION

4.1. *Electron Drift Velocity*

From (12) we see that the electron drift velocity is given simply as the ratio of the Hall field to the magnitude of the magnetic field, measured in Tesla. As a result, this value will be dependent on pressure. Our general results are given in Figure (8), where the effective drift velocity at each data point is calculated.

A sharp drop in electron drift velocity with increasing Hall field is evident. At minimum field strengths,

$\leq 150 \, \mathrm{V/m}$, velocities are at or near 10,000 m/s. There is clearly asymptotic behavior as the Hall field values approach the maximum available in this experiment, with an apparent minimum drift velocity of $\simeq 2,000 \, \mathrm{m/s}$. Theoretically, we expect this behavior, as the Hall effect is a deflection of charge carriers perpendicular to their direction of motion. As the electrons attempt to propagate from one end of the discharge column to the other, along the high voltage potential difference, they are deflected to the walls. This effectively impedes their motion and reduces their drift velocity.

Using the best fit lines we calculate a drift velocity characteristic of each pressure value, shown together with

TABLE 1
ELECTRON DRIFT VELOCITIES

Pressure (torr)	V_o (m/s)	I_D (kV)	$\boldsymbol{u}_e$ (mA)
15	1.4	0.45	$10,850 \pm 600$
18	1.6	0.75	$14,250 \pm 600$
21	1.7	0.70	$13,600 \pm 570$
24	2.1	1.00	$15,850 \pm 530$
27	1.9	0.50	$12,110 \pm 510$
30	2.1	0.65	$13,570 \pm 450$

their associated uncertainties in Table (1). Although errors decrease with increasing pressure, as expected from Figure (7), there is no obvious trend of $\boldsymbol{u}_e$ with pressure. Higher pressures have correspondingly higher charge carrier densities, and so more frequent collisions. We also expect the Hall field to go as P^{-1}, and in general would expect the drift velocity to do the same. It is possible that other effects related to changes in pressure are affecting charge carrier mobility.

4.2. *Plasma Instabilities*

Plasmas support several type of wave phenomena, including instabilities induced by certain combinations of discharge and gas parameters. Time-varying instabilities have the potential to introduce large errors into our measurements, and so a steady state is absolutely necessary. Despite these efforts, stationary structures called "striations" are evident for almost all configurations. These bands, which are visually detectable, are standing ionization waves appearing along the long axis of the plasma.

In general, striations may be both moving and stationary. They may move between the two high voltage terminals with speeds of 10^3-10^5 cm/s (Nedospasov, 1968). The electric potential can decrease stepwise instead of continuously, where potential jumps increase the electron temperature and therefore the ionization in the front of the striation. The tail of the striation has insufficient average electron energies to produce ionization, and so no visible glow is observed.

We expect that plasma instabilities will be more pronounced for certain values of the current I_D and gas pressure P. In this particular 2D parameter space there is a bounded area representing upper and low limits for the existence of striations (Nedospasov, 1968). For example, we observe quiescent operation with no visible striations at $P \simeq 25\,\text{torr}$ and $I_D \simeq 1.0\,\text{mA}$, while at a lower pressure $P \simeq 20\,\text{torr}$ striations are manifest up to nearly $I_D \simeq 2.0$ mA. Practically, this means that although we may be able to eliminate striations for certain combinations of electrical and gas parameters, it will be impossible to do so over the full range of pressures from 15 to 30 torr and currents from 0.1 to 2.5 mA.

4.3. *Density and Collision Frequencies*

The electron number density and collision frequency can also be directly calculated from the measured Hall field. Given a tube diameter of 8 mm, the cross-sectional area is $0.5\,\text{cm}^{-2}$. Discharge currents are listed for each pressure setting in Table (1). Equation (13) can then be used to calculate the number density of charge carriers. Similarly, the frequency of collisions between carriers can be calculated from Equation (14). These two results are
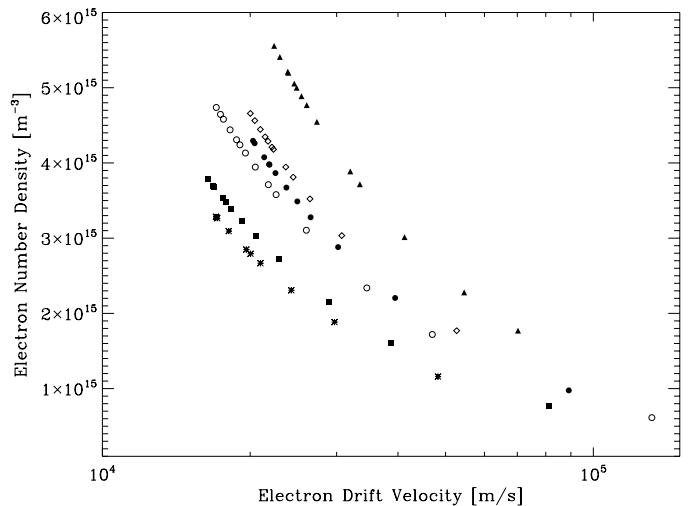

FIG. 9.— Electron number density as a function of drift velocity. As expected, the two are inversely related, where higher number densities coincide with lower drift velocities. Additionally, the density falls off rapidly with increasing carrier mobility.
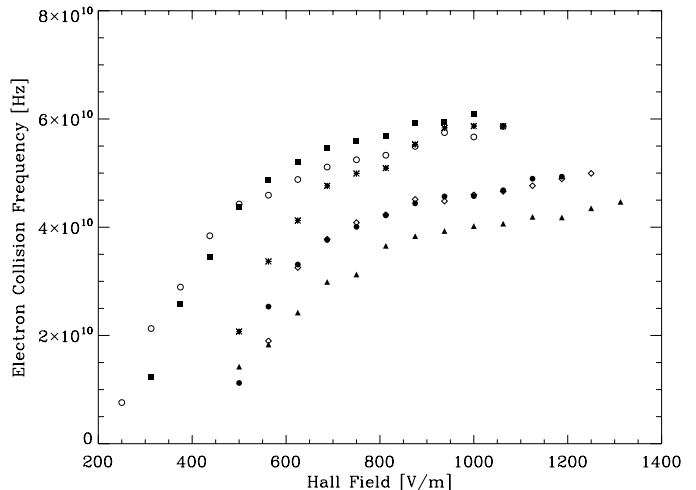

FIG. 10.— Electron collision frequency as a function of the Hall field strength. In direct parallel to the number density, we observe that the collision frequency increases asymptotically with the Hall field to a maximum value of $\simeq 6 \times 10^{10}\,\text{s}^{-1}$.

Both results are in good agreement with theoretical expectations. Higher number densities result in more collisions between charge carriers and the background medium. As each collision results in the exchange of momentum, the mobility of carriers decreases with density. At lower densities collisions occur less often and electrons are more easily able to move down the high potential gradient. That is, drift velocity is inversely proportional to number density.

4.4. *Electron Temperature*

Treating the free electrons and free ions as populations of particles with Maxwell-Boltzmann velocity distributions, an effective temperature corresponding to their average velocities can be calculated. For a weakly ionized gas, the collision frequency of (14) can be approximated as

$$\nu_q \cong n_g <\sigma v>_q \qquad (15)$$

where $<\sigma v>_q$ is the velocity averaged cross section for particle species q, and n_g is the gas density. At room temperature, the ideal gas law gives $n_g \simeq 10^{24}\,m^{-3}$ for our helium mixture. From Figure (9) the electron number density is $\simeq 10^{15}\,m^{-3}$, so the degree of ionization $n_e/n_g \simeq 10^{-10}$, verifying the weakly ionized assumption. Taking the cross section as approximately constant,

$$<\sigma v>_q \cong \sigma <|v|>_q . \qquad (16)$$

We take $\sigma = 3.8 \times 10^{-20}\,m^2$ for the helium atom, and the average thermal velocity is given by the M-B distribution as

$$<v>_q = \sqrt{\frac{8kT_q}{\pi m_q}}. \qquad (17)$$

For a given T_q, assuming exactly three translational degrees of freedom, the average energy of a free particle (such as an electron) is given by

$$E_q = \frac{1}{2}m_q <v_q^2> = \frac{1}{2}m_q \left(\frac{3kT_q}{m_q}\right) = \frac{3}{2}kT_q. \qquad (18)$$

We calculate the average speed from the collision frequency, and solve for the electron temperature T_e. The results are given in Figure (11).
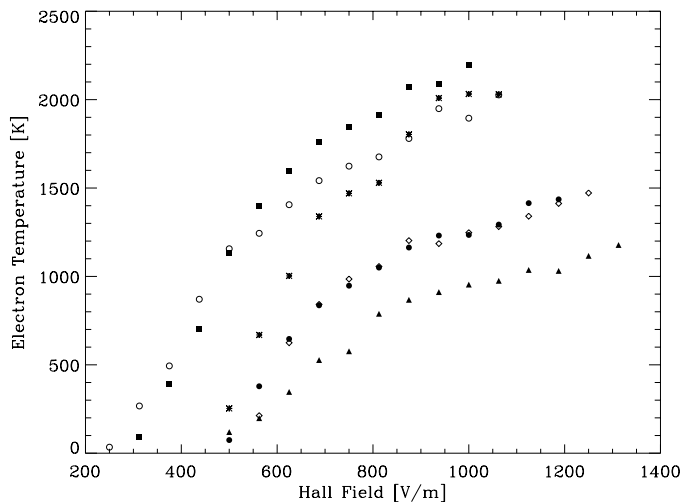

FIG. 11.— Electron temperature in Kelvin as a function of Hall field strength. The temperature increases somewhat with $\boldsymbol{E}_H$, and exhibits potentially asymptotic behavior at the highest field values. The average T_e is 1140°K, and the maximum is 2200°K.

Although the values of T_e are in general slightly lower than expected, they do increase with the Hall field strength. This is expected since the drift velocity drops and collision frequency increases with increasing Hall field. Although we might expect the velocities to be thusly decreased, leading to a lower temperature, it is the random thermal velocities which are characterized by the temperature.

The electron temperature is also significantly higher than both the ion temperature and the exterior temperature of the plasma tube. This can arise when the

ions and/or electrons have different collision rates among themselves than with each other. As a result, ions and electrons can each be in separate thermal equilibrium with associated temperatures T_i and T_e without being in thermal equilibrium with the other population group. Finally, due to the low number density of electrons, an electron temperature on the order of 10,000°K or higher does *not* mean that the walls of the tube will experience significant collisional heating at thermal velocities, which is indeed the case.

5. CONCLUSION

By first examining the physics behind the Hall effect, we determined the relations between various experimental variables and fundamental properties of interest related to the plasma discharge. We considered the specific geometry of the cylindrical discharge tube, and found that the Hall field is only half the expected value due to the effects of ambipolar diffusion.

After covering the basics of the experimental apparatus, we briefly characterized its response and that of the plasma. The discharge voltage V_o was found to be independent of the discharge current I_D, a non-Ohmic characteristic response of the plasma. By measuring the magnetic field strength as a function of magnetic current I_M, we found a small though evident hysteric effect due to the ferromagnetic material. Finally, we measured the Hall voltage and therefore the Hall field $\boldsymbol{E}_H$ as a function of magnetic field B. The response was found to be fairly linear well beyond 300 G, and we estimated general uncertainties to be approximately 30% or less.

From the Hall field measurements we determined electric drift velocities $\boldsymbol{u}_e$ between 10,000 m/s and 15,000 m/s, depending on pressure, in good agreement with the example provided. The appearance of plasma instabilities, or striations, was briefly discussed, and its impact on our measurement errors estimated as minor given appropriate precautions, e.g., assuring quiescent operation before taking data.

With only a few basic measurements we have made calculations of several plasma parameters corresponding to our helium gas discharge tube. The density of charge carriers was calculated to be of order $10^{15}\,m^{-3}$, and their collision frequency to be $\simeq 10^{10}\,s^{-1}$. Assuming a Maxwell-Boltzmann velocity distribution for the electrons allowed us to calculate an effective electron temperature $T_e \simeq 2,200$ K. This corresponds to an average energy of $\simeq 0.3$ eV, a factor of a few lower than expected. Still, it is sufficient for the tail end of the velocity distribution to provide enough energy to ionize the helium atoms in the gas, creating the plasma. We end by noting that the electrons and ions, while in thermal equilibrium within their species, need not be in thermal equilibrium with each other. As a result, and due to the low number density of electrons, temperatures greatly exceeding room temperature can be present in the plasma while the discharge tube itself is barely warm to the touch.

This experiment has provided an introductory examination of plasma physics and several interesting phenomena associated with a plasma discharge tube. Many details and subtleties remain, however, and further investigation is certainly motivated by our initial results here.

REFERENCES

Brown, S.C., *Introduction to Electrical Discharges in Gases.* Wiley, 1965.

Chen, F.F., *Plasma Physics and Controlled Fusion.* Plenum Press, 2nd ed., 1984.

Franklin, R.N., *Plasma Phenomena in Gas Discharges.* Clarendon Press, 1976.

Golant, V.E., Zhilinsky, A.P., Sakharov, I.E., & Brown, S.C., *Fundamentals of Plasma Physics.* Wiley, 1980.

Hirsh, M.N., & Oskam, J.J., eds., *Gaseous Electronics, Vol 1. "Electric discharges".* Academic Press, 1978.

Kittel, C., *Introduction to Solid State Physics.* Wiley, 4th ed., 1971.

Kittel, C., & Kroemer, H., *Thermal and Statistical Physics.* Wiley, 2nd ed., 1980.

Kunkel, W.B., *Hall Effect In A Plasma.* American Journal of Physics 49, 733, 1981.

Melissinos, A. C., & Napolitano, J., *Experiments in Modern Physics.* Academic Press, 2nd ed., 2003.

Nedospasov, A.V., *Striations.* Usp. Fiz. Nauk 94, 439-462, 1968.

Pekarek, L., *Ionization Waves (Striations) in a Discharge Plasma.* Usp. Fiz. Nauk 94, 463-500, 1968.

Taylor, J. R., *An Introduction to Error Analysis.* University Science Books, 2nd ed., 1997.